ADVANCED MATERIALS

Check for updates

Transparent, Compliant 3D Mesostructures for Precise Evaluation of Mechanical Characteristics of Organoids

*Hanjun Ryu, Yoonseok Park, Haiwen Luan, Gokhan Dalgin, Kira Jeffris,
Hong-Joon Yoon, Ted S. Chung, Jong Uk Kim, Sung Soo Kwak, Geumbee Lee,
Hyoyoung Jeong, Jihye Kim, Wubin Bai, Joohee Kim, Yei Hwan Jung, Andrew K. Tryba,
Joseph W. Song, Yonggang Huang, Louis H. Philipson, John D. Finan,* and John A. Rogers**

Recently developed methods for transforming 2D patterns of thin-film materials into 3D mesostructures create many interesting opportunities in microsystems design. A growing area of interest is in multifunctional thermal, electrical, chemical, and optical interfaces to biological tissues, particularly 3D multicellular, millimeter-scale constructs, such as spheroids, assembloids, and organoids. Herein, examples of 3D mechanical interfaces are presented, in which thin ribbons of parylene-C form the basis of transparent, highly compliant frameworks that can be reversibly opened and closed to capture, envelop, and mechanically restrain fragile 3D tissues in a gentle, nondestructive manner, for precise measurements of viscoelastic properties using techniques in nanoindentation. Finite element analysis serves as a design tool to guide selection of geometries and material parameters for shape-matching 3D architectures tailored to organoids of interest. These computational approaches also quantitate all aspects of deformations during the processes of opening and closing the structures and of forces imparted by them onto the surfaces of enclosed soft tissues. Studies of cerebral organoids by nanoindentation show effective Young's moduli in the range from 1.5 to 2.5 kPa depending on the age of the organoid. This collection of results suggests broad utility of compliant 3D mesostructures in noninvasive mechanical measurements of millimeter-scale, soft biological tissues.

1. Introduction

3D mesostructures are of widespread interest because, by comparison to conventional 2D counterparts, they offer expanded and enhanced functional possibilities in areas ranging from biomedical devices,[1–7] electronic devices,[8–13] and sensors.[14–17] Although fabrication techniques based on 3D printing,[18–20] self-rolling,[21–23] and origami/kirigami[24–26] offer utility in this context, each has some set of limitations in materials compatibility, structural diversity, resolution and patterning speed. Alternative schemes based on mechanical assembly begin with formation of 2D thin-film structures using any of a wide variety of sophisticated lithographic approaches applied to the most advanced functional materials. Controlled processes of buckling transform these 2D precursors into open-architecture 3D geometries in a high-speed, parallel fashion with versatility in materials (semiconductors, metals, insulators of both

Dr. H. Ryu, Dr. Y. Park, Dr. H. Luan, Dr. H.-J. Yoon, T. S. Chung,
Dr. J. U. Kim, Dr. S. S. Kwak, Dr. G. lee, Dr. H. Jeong,
Dr. J. Kim, Dr. J. Kim, Dr. A. K. Tryba, Prof. J. A. Rogers
Querrey Simpson Institute for Bioelectronics
Northwestern University
Evanston, IL 60208, USA
E-mail: jrogers@northwestern.edu
Dr. H. Ryu, Dr. H.-J. Yoon, Dr. S. S. Kwak, Dr. J. Kim
School of Advanced Materials Science and Engineering
Sungkyunkwan University (SKKU)
Suwon 16419, Republic of Korea
Dr. G. Dalgin
Section of Adult and Pediatric Endocrinology
Diabetes and Metabolism
Kovler Diabetes Center
The University of Chicago
Chicago, IL 60637, USA

K. Jeffris, Prof. J. D. Finan
Department of Mechanical and Industrial Engineering
University of Illinois at Chicago
Chicago, IL 60607, USA
E-mail: jdfinan@uic.edu
T. S. Chung, J. W. Song, Prof. J. A. Rogers
Department of Biomedical Engineering
Northwestern University
Evanston, IL 60208, USA
J. W. Song
Center for Bio-Integrated Electronics
Northwestern University
Evanston, IL 60208, USA
J. U. Kim
School of Chemical Engineering
Sungkyunkwan University (SKKU)
Suwon 16419, Republic of Korea
Prof. W. Bai
Department of Applied Physical Sciences
University of North Carolina at Chapel Hill
Chapel Hill, NC 27599, USA

organics and inorganics), layer thicknesses (from millimeters to atomic dimensions), feature sizes (from nanometers to centimeters) and layouts (open or closed architectures of ribbons, beams, membranes, and others).[27–30]

These capabilities in materials, devices, and 3D assembly methods are highly relevant in the context of biological systems, where 3D design features are ubiquitous. Miniaturized 3D tissue constructs are of particular interest, due to their increasing roles in biological research. Here, human induced pluripotent stem cells grown into 3D cell cultures serve as model systems of vital organs, from the heart to the brain, the spinal cord, the liver, the gut, and others. Brain tissues of such types, referred to as cerebral organoids,[31,32] can be used as platforms for studies of neural differentiation, regeneration, communication, development and disease. Recent work demonstrates the ability of 3D constructs, called 3D multifunctional mesoscale frameworks (3D MMFs), to serve as electrical, thermal, optical, and electrochemical interfaces to these systems.[33] Many biological properties and behaviors depend also on mechanical cues and characteristics, at the level of individual cells and collections of them and their interactions with surrounding materials. Relevant effects include aspects of cell formation, functionality, motility, differentiation, and others.[34] Cytoskeletal, nuclear, or extracellular matrix changes contribute to changes in the Young's modulus of organoids, as indicators of abnormalities and mutations.[35,36] Direct characterization of

the mechanical properties with probes, such as nanoindenters or tips for atomic force microscopy (AFM) can, however, be challenging because these structures move freely in cell culture media without positional fixation.[37] Hydrogels can be useful as concave cavities shape-matched to the organoids,[38,39] but their fabrication can be cumbersome[35,40] and they often do not maintain the positions of the organoids during cell culture medium exchange, introduction of drugs or other manipulations. Microwell arrays are capable of separating organoids, but organoids randomly rotate and move in such wells.

Herein, we introduce a soft and transparent class of 3D MMF designed to gently envelop and mechanically constrain organoids in ways that facilitate mechanical evaluations without damage. A photolithography-based fabrication process yields complex 2D precursors with micrometer thicknesses in a variety of material options such as parylene-C, polyimide (PI), and more, with straightforward possibilities for integrating electronic, optoelectronic and biochemical sensing functions.[33] These 3D structures can be reversibly deformed by laterally stretching a thin elastomeric substrate, as a mechanism to open and close the system around an organoid in a controlled manner. Finite element analysis (FEA) serves as a guide to select 3D layouts that match the geometries of organoids of interest and to grasp them with minimal force. Calcein-AM/propidium iodide cell viability assays and optical microscopy studies reveal an absence of acute damage to the tissues. Techniques of nanoindentation can be applied directly to organoids while enclosed in these frameworks, for accurate and repeated measurements of force/displacement data. The effective Young's moduli determined from these measurements quantitatively define the dependence on age, indentation depths, indentation speeds. Changes in mechanical characteristics induced by controlled exposure to blebbistatin and ethanol highlight options in studies of responses to the chemical environment. The results suggest broad utility in precise, nondestructive mechanical testing of small-scale biological tissues.

Prof. Y. H. Jung
Department of Electronic Engineering Hanyang University
Seoul 04763, Republic of Korea

Dr. A. K. Tryba
Section of Pediatric Neurology
Department of Pediatrics
The University of Chicago
Chicago, IL 60637, USA

Prof. Y. Huang, Prof. J. A. Rogers
Department of Mechanical Engineering
Northwestern University
Evanston, IL 60208, USA

Prof. Y. Huang
Department of Civil and Environmental Engineering
Northwestern University
Evanston, IL 60208, USA

Prof. Y. Huang, Prof. J. A. Rogers
Department of Materials Science and Engineering
Northwestern University
Evanston, IL 60208, USA

Prof. L. H. Philipson
Department of Medicine and Kovler Diabetes Center
The University of Chicago
Chicago, IL 60637, USA

Prof. J. A. Rogers
Department of Chemistry
Northwestern University
Evanston, IL 60208, USA

Prof. J. A. Rogers
Department of Electrical and Computer Engineering
Northwestern University
Evanston, IL 60208, USA

Prof. J. A. Rogers
Departments of Neurological Surgery
Feinberg School of Medicine
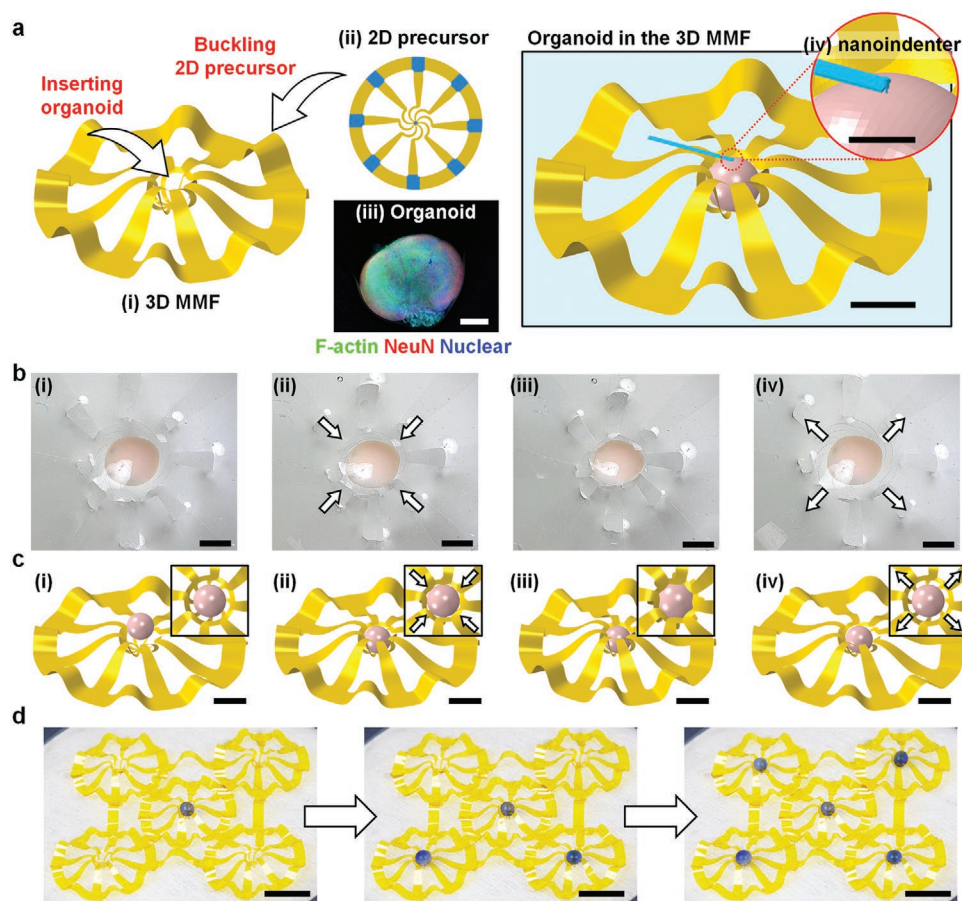Northwestern University
Chicago, IL 60611, USA

2. Results and Discussion

Figure 1a shows a schematic illustration of a 3D MMF designed for these purposes, and of steps in opening and closing this structure around a cerebral organoid with an approximately spherical shape. The design of the 2D precursor, the bonding sites and the prestrain field are the main factors that determine the 3D geometry; gravity and buoyancy have a negligible effect when the organoid and 3D MMF are immersed in a cell culture medium. Here, the 2D precursor consists of a thin ($\approx$13 µm) layer of parylene-C (para-xylylene dimer, Specialty Coating Systems Inc., USA) patterned by photolithography and reactive-ion etching. Electron beam evaporation through a shadow mask forms square pads of Ti/SiO$_2$ (10/100 nm in thickness) at selected regions on the bottom side of the 2D precursor, to define sites of bonding to a biaxially stretched (30%) thin ($\approx$1.2 mm in thickness) substrate of poly(dimethylsiloxane) (PDMS, Sylgard 184, Dow, USA; 20:1). In one example, the 2D precursor includes a radially symmetric collection of eight "wings" with widths of 170 µm and a section that twists into a curved structure with inner and outer radii of 720 µm ($R_{in,1}$)

**ADVANCED
SCIENCE NEWS**

www.advancedsciencenews.com

**ADVANCED
MATERIALS**

www.advmat.de

Figure 1. a) Schematic image of an organoid in a 3D MMF. Scale bar: 2 mm. i) 3D MMF after buckling. ii) 2D precursor, with bonding sites indicated in blue. iii) Immunohistochemistry for F-actin (green), NeuN (red), and Nuclear (blue) in a cerebral organoid. scale bar: 0.5 mm. iv) Location of nanoindenter on an organoid for indentation. scale bar: 0.5 mm. b) Optical microscopy images of the reversible process of closing and opening the 3D MMF. i) Opened 3D MMF with an organoid, ii) releasing the substrate to close, iii) fully closed 3D MMF with an inserted organoid, iv) opened 3D MMF after stretching the substrate. Scale bar: 1 mm. c) FEA results at different stages of the process of inserting a cerebral organoid into the 3D MMF; from left: i) slightly stretch the substrate to open the 3D MMF and insert organoid ($\varepsilon_{appl} = 10\%$), ii) slightly release the substrate to close 3D MMF ($\varepsilon_{appl} = 5\%$); iii) fully release the substrate to close the 3D MMF ($\varepsilon_{appl} = 0\%$), and iv) slightly stretch the substrate to open the 3D MMF and remove organoid ($\varepsilon_{appl} = 10\%$). Scale bar: 2 mm. The inset figures are top-view images of the corresponding FEA results. d) Arrays of 3D MMFs with similar dimensions, for high-throughput screening; from left: after inserting a single sphere into the center 3D MMF, after inserting two additional spheres in the bottom pair of 3D MMFs, and after inserting two additional spheres in the top pair of 3D MMFs. Scale bar: 2 cm.

and 920 µm ($R_{out,1}$), respectively, terminating with a width of 440 µm. The widths of the straight sections increase linearly from 440 µm to 1 mm along a length of 3.8 mm (see Figure S1, Method, Supporting Information). Allowing the substrate to relax to its unstretched state leads to compressive forces on the 2D precursor at the bonding locations. The result leads to delamination at the nonbonded regions, with translational and rotational motions out of the plane, thereby transforming the system into a 3D structure. The 3D MMF uses a 35 mm cell culture plate (or larger) to contain the cell culture medium. Stretching or relaxing the substrate opens or closes, respectively, the system to allow for manual insertion or removal of an organoid (Figure 1b; see Figure S2 and Movie S1, Supporting Information). FEA results demonstrate this process of inserting an organoid into a 3D MMF (see Figure 1c). Figure 1d demonstrates the scalability of the process and the ability to locally open/close individual 3D MMFs in a large array by vertically pressing the bottom elastic substrate of each 3D MMF, fabricated

in this case from a 12.5 µm thick substrate of PI (Dupont, USA) using laser manufacturing process to simplify the fabrication process. Currently, five such frameworks is the maximum number possible in a single system due to practical considerations based on the size of the stretchable substrate, the design of the mechanical stretcher, and area of the 2D precursor.

Procedures for forming the cerebral organoids follow protocols by Lancaster (see Figure 1a(iii))[41] using an induced pluripotent stem cell (iPSC) line with confirmed expression of pluripotency markers NANOG and OCT4 (see Figure S3a,b, Supporting Information) and ability to differentiate into three germ layers; PAX6 expressing ectoderm, BRA expressing mesoderm, and FOXA2 expressing endoderm (see Figure S3c–e, Supporting Information). The developing organoids show typical morphology (see Figure S3f–I, Supporting Information) and expression of the neural stem cell marker SOX2 and forebrain marker FOXG1 (see Figure S3j,k, Supporting Information).
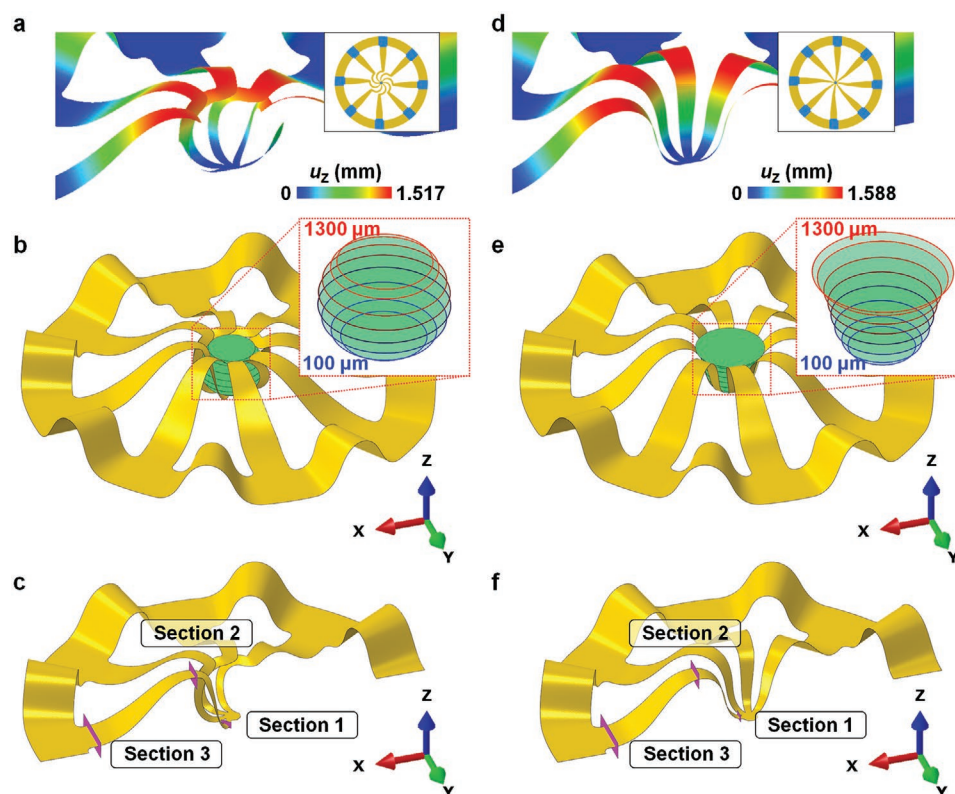
ADVANCED
SCIENCE NEWS
www.advancedsciencenews.com

**ADVANCED
MATERIALS**
www.advmat.de

Figure 2. a,d) FEA results of geometries and out-of-plane displacements (u_z) associated with 3D MMFs with twisted (a) and straight (d) designs. The insets show the layouts of the 2D precursors, with bonding sites indicated in blue. b,e) The sectional diameters of the spaces defined by these structures at eight different heights for the twisted (b) and straight (e) designs. c,f) Illustration of the locations for reported bending stiffnesses for the twisted (c) and straight (f) designs.

Figure 2 summarizes essential geometrical and mechanical properties features of several different 3D MMFs. The version with curved wings forms: 1) a twisted structure with a peak rotation angle of 40.4° and large convex curvature, and 2) a gradual concave curvature, sequentially, to create an enclosed space in an approximately spherical shape (see Figure 2a). Circular curves drawn within the space defined by the structure, oriented parallel to the substrate, have diameters of 1162, 1420, 1676, 1784, 1770, 1670, 1458, and 1294 μm at heights of 100, 200, 400, 600, 800, 1000, 1200, and 1300 μm, respectively, above the substrate (see Figure 2b; and Figure S4, Supporting Information). This twisted design forms a large volume within the structure and a shape accurately tailored for spherical organoids, as differentiated from the less optimal, straight wing design as previously reported. The bending stiffness at the point of the central bonding site is 8.84×10^{-11} N m² (Section 1), increasing to 2.46×10^{-10} N m² (Section 2) and finally to 5.23×10^{-10} N m² (Section 3) (see Figure 2c). The design with straight wings forms: 1) a gradual convex curvature from the central bonding site, 2) a linear region, and 3) a gradual concave curvature to define an approximately conical enclosed space (see Figure 2d). This space is characterized by diameters of 912, 1080, 1278, 1386, 1474, 1588, 1764, and 1906 μm at heights of 100, 200, 400, 600, 800, 1000, 1200, and 1300 μm, respectively, above the substrate (see Figure 2e; and Figure S4, Supporting Information). The bending stiffness at the point of the central bonding site is 8.59×10^{-11} N m² (Section 1), increasing

to 2.79×10^{-10} N m² (Section 2) and finally to 5.23×10^{-10} N m² (Section 3), similar to the twisted system (see Figure 2f). Simulations in Figure S5 (Supporting Information) indicate that the twisted structure fixes a spherical organoid with a diameter of 1.7 mm under a maximum compressive stress of 824 Pa from top to bottom; the straight structure cannot hold the same type of organoid due to insufficient maximum lateral compressive stress (183 Pa) and effects of buoyancy and minute fluid flows, thereby leading to uncontrolled slight motions.

Figure 3 shows the results of FEA for the out-of-plane displacements as well as the distributions of strain and stress for 3D MMFs and enclosed organoids. Design choices here match those of the shapes and sizes of the organoids. Spherical organoids with diameters at least 1.6 mm can fit into cavities defined by 3D structures with maximum heights of 1.5 mm (Figure 3a). According to the results of Figure 3b, the strains that occur in the 3D MMF are less than limits of plastic deformation and fracture of the parylene-C.[42] An organoid with a diameter of 1.6 mm, which is the smallest size that can fit into the 3D MMF, is free from any stress induced by the 3D MMF (see Figure 3b,3c; and Figure S6, Supporting Information). Figure 3d shows an example of an ellipsoidal organoid ($a = 0.9$ mm, $b = 0.9$ mm, $c = 0.75$ mm) with the minimum size for the 3D MMF. The dimensions of this organoid ensure an absence of forced contact with the 3D MMF, such that the strain distribution in the 3D MMF is unaltered and the organoid is free from stresses (see Figure 3e,f; and Figure S6,
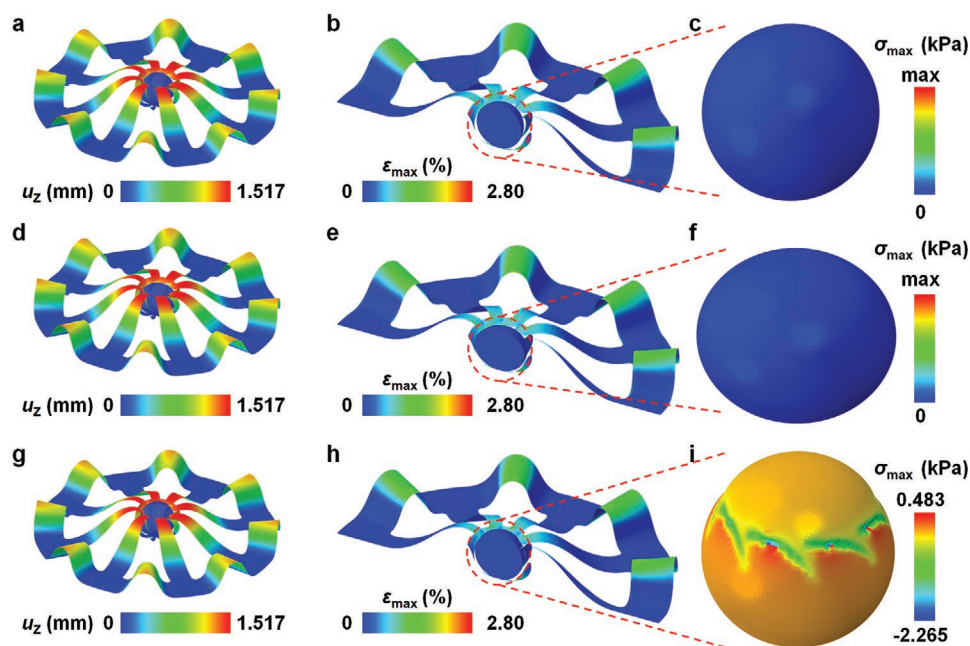
**ADVANCED
SCIENCE NEWS**
www.advancedsciencenews.com

**ADVANCED
MATERIALS**
www.advmat.de

Figure 3. FEA results for the out-of-plane displacements (u_z), and the distribution of strains and stresses of 3D MMFs enclosing a 1.6 mm diameter spherical organoid (a–c), an ellipsoidal organoid ($a = 0.9$ mm, $b = 0.9$ mm, $c = 0.75$ mm) (d–f), and a 1.7 mm diameter spherical organoid (g–i).

Supporting Information). Figure 3g demonstrates the case of insertion of a spherical organoid with a diameter of 1.7 mm, where stresses (up to ≈2 kPa in compression) form at the areas

of contact (see Figure 3h,i; and Figure S6, Supporting Information). In general, a 3D MMF can hold an organoid with a diameter up to ≈0.1 mm larger than the design point without
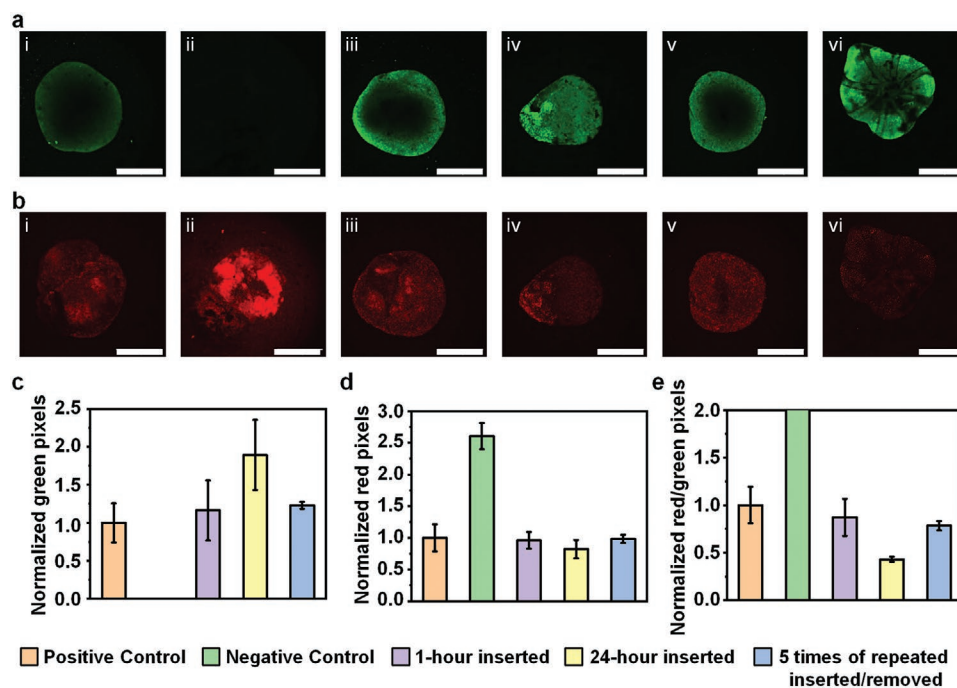

Figure 4. a) Calcein AM and b) propidium iodide stained fluorescence images of organoids associated with: (i) a positive control, in the form of an organoid not in a 3D MMF; (ii) a negative control, in the form of an organoid exposed to a toxic drug; (iii) an organoid one hour after insertion into a 3D MMF followed by removal; (iv) an organoid 24 h after insertion into a 3D MMF followed by removal; (v) an organoid after five cycles of insertion and removal from a 3D MMF; and vi) an organoid 24 h after insertion into a 3D MMF, while still in the 3D MMF. Scale bar: 1 mm, 164-day-aged organoids. c–e) Normalized numbers of pixels for Calcein AM (green) (c) and PI (red) (d), and for ratios of PI and Calcein AM (e). $n = 3$, 164-day-aged organoids. The error bars correspond to standard deviations.

**ADVANCED
SCIENCE NEWS**
www.advancedsciencenews.com

**ADVANCED
MATERIALS**
www.advmat.de

significant deformation and damage.[43] Linear scaling (expansion or contraction) of the 2D framework renders 3D MMFs with different sizes to match requirements (see Figure S7, Supporting Information). For a larger spherical organoid with a diameter of 2.2 mm, a 3D MMF, linearly scaled up by a factor of 2.2/1.7, can hold an organoid with similar strain/stress levels (see Figure 3g–i; and Figure S8, Supporting Information).

Studies of cytotoxicity involve Calcein AM/PI as a stain for viable/dead cells for five different conditions and organoid groups (see **Figure 4**). Figure 4a shows results of Calcein AM staining of spherical organoids with diameters of ≈1.7 mm inserted into a 3D MMF with the twisted design. Figure 4b highlights findings associated with PI staining, including cases of: i) a positive control (an organoid not in a 3D MMF), ii) a negative control (an organoid exposed to a toxic drug), iii) an organoid 1 h after insertion into a 3D MMF followed by removal, iv) an organoid 24 h after insertion into a 3D MMF followed by removal, v) an organoid after five cycles of insertion and removal from a 3D MMF, and vi) an organoid 24 h after insertion into a 3D MMF, while still in the 3D MMF. Comparisons of bright-field images before insertion and fluorescence images after, which show that the organoids remain intact for all insertion conditions with no evidence of fragmentation or rupture (see Figure S9, Supporting Information). The positive control shows mild green and red fluorescence; the negative control shows zero green fluorescent and a high red fluorescence. The cases of (iii–v) show similar levels of green and red fluorescence, consistent with absence of damage (see Figure 4c–e). The ratio of PI and Calcein AM of the negative control is not well defined due to the absence of green pixels. Quantitative real time polymerase chain reaction (qRT-PCR) measures 4 target genes (FOXG1, RBFOX3/NEUN, S100B, TUJ1/TUBB3) and two reference genes (18S, RPL37A) in each of these organoids to quantify changes in gene expression after insertion into 3D MMF. The Control group (n = 4) maintains in dishes with 3D MMF but not inserted, and the experimental group (n = 3) maintains in 3D MMF for 24 h. The relative change in expression of each target gene is computed by the delta–delta CT method, and the results show similar tendencies regardless of the reference genes (see Tables 1 and 2; and Table S1, Supporting Information). FOXG1 is relatively insensitive to insertion; RBFOX3/NEUN significantly increases. The transparency of the 3D MMF (85% across the visible; see Figure S10, Supporting Information) facilitates these and other forms of optical assays (see Figure 4a(vi),b(vi)).

Figure 5 highlights measurements of mechanical properties of cerebral organoids held in 3D MMFs with the twisted geometry, while immersed in cell culture media. The tip of the nanoindenter (Piuma nanoindenter, Optics 11, The Netherlands) establishes contact to the organoid through the exposed top area of the structure. The elastic modulus (E) of the organoid can be derived from application of the Hertz model[44,45]

$$E = \frac{3(1-\nu^2)P}{4R^{1/2}h^{3/2}} \tag{1}$$

where ν is Poisson's ratio of the indenter, P is the load, R is the radius of the spherical indenter tip, h is the penetration depth. The effective Young's modulus of the 3D MMF is

Table 1. Effect of inserting an organoid into a 3D MMF on gene expression, using 18S as the reference gene. Statistical significance was calculated using the Benjamini–Hochberg procedure.

Gene	Type	Fold change due to Insertion	P-value
18S	Selected control	1	
FOXG1	Target	1.0932	0.7865
RBFOX3/NEUN	Target	2.6647	0.0016
RPL37A	Candidate control	1.0864	0.4111
S100B	Target	0.2605	0.0926
TUJ1/TUBB3	Target	1.6746	0.0926

≈10 kPa around the top area, and ≈7 kPa near the middle wing area. These values are significantly less than those of flat 1%, 2%, and 4% agarose gel continuums (see Figure S11, Supporting Information). The force–distance curves collected in this manner have much less noise and exhibit much clearer repulsive force behaviors than those obtained from organoids without constraint (see Figure 5a; and Figure S12, Supporting Information). A 171-day-aged organoid shows an effective Young's modulus of 2.2 ± 0.1 kPa, consistent with previous AFM studies.[35,45–47] Attempts to measure the Young's modulus of the same organoid on a flat polymer substrate yield values <1 kPa, limited by poor accuracy in the force–distance data that follows from lateral movements of the organoid during the measurement. Figure 5b shows the effective Young's modulus of organoids with ages from 63 to 171 days. The diameters of the organoids increase with age, from 1.4 to 2.2 mm. The middle-aged organoids (between 60 and 100 days) show effective Young's moduli of ≈1.5–2 kPa. Mature organoids (over 100 days) have moduli of ≈2–2.5 kPa (see Figure S3f–i, Supporting Information). Data from indentation depths between 3.5 and 12 µm have slightly different types of force-distance curves, with moduli from ≈1.4 to ≈2.4 kPa with increasing depth (see Figure 5c).[48] The effective modulus also depends on indentation speed, changing monotonically from 1.3 to 3.3 kPa for speeds from 1 to 75 µm s^{-1} (see Figure 5d).[49]

The open architecture of these 3D MMFs allows direct studies of the effects of drugs on modulus, following from their influence on actin fibers, myosin filaments, and cytoskeletons. Examples reported here include introduction of 10 × 10^{-6} M of blebbistatin[50] and 50 × 10^{-3} M of ethanol,[51] as representative chemistries that reduce and enhance the modulus without

Table 2. Effect of inserting an organoid into a 3D MMF on gene expression, using RPL37A as the reference gene. Statistical significance was calculated using the Benjamini–Hochberg procedure.

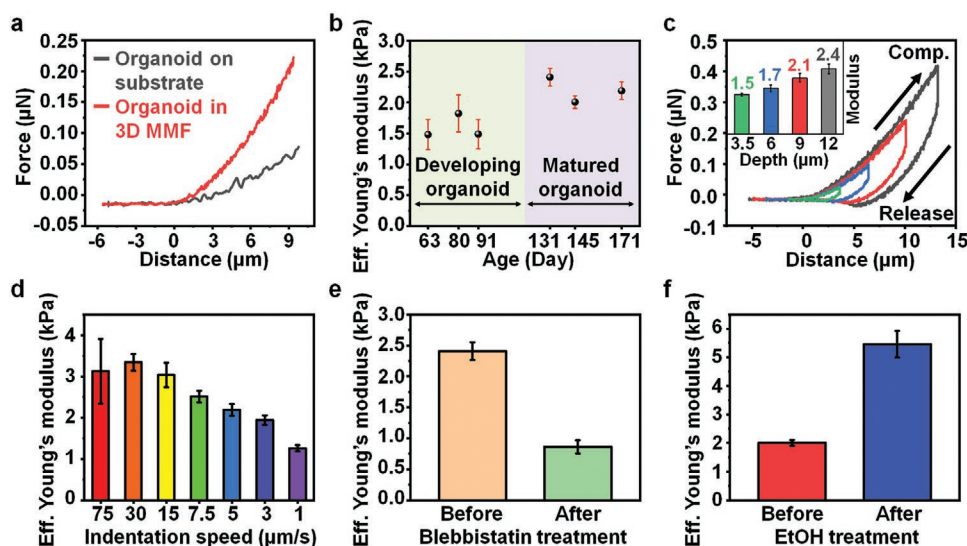| Gene	Type	Fold change due to insertion	P-value
18S	Candidate control	0.9099	0.4121
FOXG1	Target	0.9683	0.9385
RBFOX3/NEUN	Target	2.368	0.0194
RPL37A	Selected control	1	
S100B	Target	0.2244	0.2383
TUJ1/TUBB3	Target	1.4489	0.3524

Figure 5. a) Force–distance curves and effective Young's modulus values of organoids and the 3D MMF. b) Effective Young's modulus of organoids with different ages measured in a 3D MMF with an indentation speed of 5 μm s^{-1}. c) Force–distance curves for indentation depths of 3.5, 6, 9, and 12 μm at speeds of 5 μm s^{-1}. The inset graph shows the effective Young's modulus from data collected to depths of 3.5 (green), 6 (blue), 9 (red), and 12 μm (black). d) Effective Young's modulus values determined at different indentation speeds to depths of 12 μm. e,f) Effective Young's modulus values before and after exposure to blebbistatin (10×10^{-6} M) for 2 h (e) and exposure to ethanol (50×10^{-3} M) for 2 h (f). The error bars correspond to one standard deviation. Number of indentations: >15.

significant toxicity (see Figure S13, Supporting Information). Figure 5e presents data that show that the effective Young's modulus decreases from ≈2.4 to 0.9 kPa after 2 h exposure to 10×10^{-6} M of blebbistatin, consistent with expected disruption of myosin contractility and actin polymerization.[52] The effective Young's modulus increases from ≈2 to 5.5 kPa after 2 h exposure to 50×10^{-3} M of ethanol treatment (see Figure 5f), consistent with the promotion of phosphorylation of myosin motor proteins[53,54] and consequent increase in tension in actin fibers.[55]

While nanoindentation is the primary assay in this study, many other important and popular assays will be easier to apply to organoids when they are immobilized with a 3D MMF. For example, the widely use patch clamp electrophysiological assay also requires pressing a probe gently against the sample and this is difficult to do when the sample is mobile. Also, high content time series imaging typically involves cycling through locations on the assumption that previously viewed samples will be at the previous viewed location when it is time to view them again. 3D MMFs can position organoids stably and consistently to make these and other assays more reliable and easier to apply. Therefore, 3D MMFs are likely to find many powerful applications in the study of brain and other types of organoids.

3. Conclusion

The compliant and transparent 3D MMFs introduced here provide simple but useful function in spatially constraining organoids for purposes of mechanical characterization. Lateral stretching of a thin elastomeric substrate provides a convenient means for opening and closing these 3D structure to facilitate insertion and removal of organoids for testing. A twisted design in the 3D framework yields a highly spherical

cavity with dimensions that can be matched precisely to organoids of interest. FEA techniques serve as design tools to allow proper selection of 2D precursor geometries and to minimize mechanical stresses on enclosed organoids. Detailed studies indicate that organoids can be released from these constructs nondestructively. Nevertheless, the possibility that insertion into the 3D MMF might perturb gene expression cannot be excluded at this time. Also, 3D MMF-induced cellular compression can possibly stimulate mechanosensitive pathways that will alter cell behavior. Measurements indicate that organoids of various ages and sizes have different characteristic Young's moduli, and that the depths and speeds of indentation can influence the apparent values, consistent with expectation and prior literature studies. The open architecture designs allow free diffusive and forced convective access to the surfaces of the organoids, as demonstrated through studies of the effects of blebbistatin and ethanol on the mechanical properties. This collection of results suggests that techniques in controlled mechanical buckling provide access to 3D mesostructures with applications as bio-interfaces to organoids and, by extensions, other small-scale tissue constructs for fundamental and applied study.

Supporting Information

Supporting Information is available from the Wiley Online Library or from the author.

Acknowledgements

Conflict of Interest

The authors declare no conflict of interest.

Data Availability Statement

The data that support the findings of this study are available from the corresponding author upon reasonable request.

Keywords

3D mesostructures, mechanical buckling, organoids, viscoelastic properties, Young's modulus

[1] X. Dai, W. Zhou, T. Gao, J. Liu, C. M. Lieber, *Nat. Nanotechnol.* **2016**, *11*, 776.

[2] X. Liu, H. Yuk, S. Lin, G. A. Parada, T. C. Tang, E. Tham, C. de la Fuente-Nunez, T. K. Lu, X. Zhao, *Adv. Mater.* **2018**, *30*, 1704821.

[3] B. Tian, J. Liu, T. Dvir, L. Jin, J. H. Tsui, Q. Qing, Z. Suo, R. Langer, D. S. Kohane, C. M. Lieber, *Nat. Mater.* **2012**, *11*, 986.

[4] R. Feiner, S. Fleischer, A. Shapira, O. Kalish, T. Dvir, *J. Controlled Release* **2018**, *281*, 189.

[5] T. G. Leong, C. L. Randall, B. R. Benson, N. Bassik, G. M. Stern, D. H. Gracias, *Proc. Natl. Acad. Sci. USA* **2009**, *106*, 703.

[6] M. S. Mannoor, Z. Jiang, T. James, Y. L. Kong, K. A. Malatesta, W. O. Soboyejo, N. Verma, D. H. Gracias, M. C. McAlpine, *Nano Lett.* **2013**, *13*, 2634.

[7] G. Rijal, W. Li, *Sci. Adv.* **2017**, *3*, e1700764.

[8] Y. Park, H. Luan, K. Kwon, S. Zhao, D. Franklin, H. Wang, H. Zhao, W. Bai, J. U. Kim, W. Lu, J. H. Kim, Y. Huang, Y. Zhang, J. A. Rogers, *Adv. Funct. Mater.* **2019**, *29*, 1903181.

[9] D. Grimm, C. C. Bof Bufon, C. Deneke, P. Atkinson, D. J. Thurmer, F. Schaffel, S. Gorantla, A. Bachmatiuk, O. G. Schmidt, *Nano Lett.* **2013**, *13*, 213.

[10] W. Liu, Z. Chen, G. Zhou, Y. Sun, H. R. Lee, C. Liu, H. Yao, Z. Bao, Y. Cui, *Adv. Mater.* **2016**, *28*, 3578.

[11] F. Liu, Y. Chen, H. Song, F. Zhang, Z. Fan, Y. Liu, X. Feng, J. A. Rogers, Y. Huang, Y. Zhang, *Small* **2019**, *15*, 1804055.

[12] D. Yan, J. Chang, H. Zhang, J. Liu, H. Song, Z. Xue, F. Zhang, Y. Zhang, *Nat. Commun.* **2020**, *11*, 1180.

[13] H. Fu, K. Nan, W. Bai, W. Huang, K. Bai, L. Lu, C. Zhou, Y. Liu, F. Liu, J. Wang, M. Han, Z. Yan, H. Luan, Y. Zhang, Y. Zhang, J. Zhao, X. Cheng, M. Li, J. W. Lee, Y. Liu, D. Fang, X. Li, Y. Huang, Y. Zhang, J. A. Rogers, *Nat. Mater.* **2018**, *17*, 268.

[14] S.-Y. Wu, C. Yang, W. Hsu, L. Lin, *Microsyst. Nanoeng.* **2015**, *1*, 2015013.

[15] S. Z. Guo, K. Qiu, F. Meng, S. H. Park, M. C. McAlpine, *Adv. Mater.* **2017**, *29*, 1701218.

[16] J. T. Muth, D. M. Vogt, R. L. Truby, Y. Menguc, D. B. Kolesky, R. J. Wood, J. A. Lewis, *Adv. Mater.* **2014**, *26*, 6307.

[17] P.-K. Yang, Z.-H. Lin, K. C. Pradel, L. Lin, X. Li, X. Wen, J.-H. He, Z. L. Wang, *ACS Nano* **2015**, *9*, 901.

[18] X. Wang, M. Jiang, Z. Zhou, J. Gou, D. Hui, *Composites, Part B* **2017**, *110*, 442.

[19] Z. Chen, Z. Li, J. Li, C. Liu, C. Lao, Y. Fu, C. Liu, Y. Li, P. Wang, Y. He, *J. Eur. Ceram.* **2019**, *39*, 661.

[20] J. Z. Gul, M. Sajid, M. M. Rehman, G. U. Siddiqui, I. Shah, K. H. Kim, J. W. Lee, K. H. Choi, *Sci. Technol. Adv. Mater.* **2018**, *19*, 243.

[21] S. Janbaz, R. Hedayati, A. A. Zadpoor, *Mater. Horiz.* **2016**, *3*, 536.

[22] Z. Zhang, K. G. Demir, G. X. Gu, *Int. J. Smart Nano Mater.* **2019**, *10*, 205.

[23] T. B. Aigner, C. Haynl, S. Salehi, A. O'Connor, T. Scheibel, *Mater. Today Bio.* **2020**, *5*, 100042.

[24] K. Bertoldi, V. Vitelli, J. Christensen, M. van Hecke, *Nat. Rev. Mater.* **2017**, *2*, 17066.

[25] A. Oyefusi, J. Chen, *Angew. Chem., Int. Ed.* **2017**, *56*, 8250.

[26] X. Ning, X. Wang, Y. Zhang, X. Yu, D. Choi, N. Zheng, D. S. Kim, Y. Huang, Y. Zhang, J. A. Rogers, *Adv. Mater. Interfaces* **2018**, *5*, 1800284.

[27] Y. Liu, X. Wang, Y. Xu, Z. Xue, Y. Zhang, X. Ning, X. Cheng, Y. Xue, D. Lu, Q. Zhang, F. Zhang, J. Liu, X. Guo, K. C. Hwang, Y. Huang, J. A. Rogers, Y. Zhang, *Proc. Natl. Acad. Sci. USA* **2019**, *116*, 15368.

[28] Z. Yan, M. Han, Y. Yang, K. Nan, H. Luan, Y. Luo, Y. Zhang, Y. Huang, J. A. Rogers, *Extreme Mech. Lett.* **2017**, *11*, 96.

[29] H. Luan, X. Cheng, A. Wang, S. Zhao, K. Bai, H. Wang, W. Pang, Z. Xie, K. Li, F. Zhang, Y. Xue, Y. Huang, Y. Zhang, *ACS Appl. Mater. Interfaces* **2019**, *11*, 3482.

[30] S. Lim, H. Luan, S. Zhao, Y. Lee, Y. Zhang, Y. Huang, J. A. Rogers, J.-H. Ahn, *Adv. Mater.* **2020**, *32*, 2001303.

[31] T. Kadoshima, H. Sakaguchi, T. Nakano, M. Soen, S. Ando, M. Eiraku, Y. Sasai, *Proc. Natl. Acad. Sci. USA* **2013**, *110*, 20284.

[32] M. A. Lancaster, M. Renner, C. A. Martin, D. Wenzel, L. S. Bicknell, M. E. Hurles, T. Homfray, J. M. Penninger, A. P. Jackson, J. A. Knoblich, *Nature* **2013**, *501*, 373.

[33] Y. Park, C. K. Franz, H. Ryu, H. Luan, K. Y. Cotton, J. U. Kim, T. S. Chung, S. Zhao, A. Vazquez-Guardado, D. S. Yang, K. Li, R. Avila, J. K. Phillips, M. J. Quezada, H. Jang, S. S. Kwak, S. M. Won, K. Kwon, H. Jeong, A. J. Bandodkar, M. Han, H. Zhao, G. R. Osher, H. Wang, K. Lee, Y. Zhang, Y. Huang, J. D. Finan, J. A. Rogers, *Sci. Adv.* **2021**, *7*, eabf9153

[34] D. Di Carlo, *J. Lab. Autom.* **2012**, *17*, 32.

[35] E. Karzbrun, A. Kshirsagar, S. R. Cohen, J. H. Hanna, O. Reiner, *Nat. Phys.* **2018**, *14*, 515.

[36] A. Dominijanni, M. Devarasetty, S. Soker, *iScience* **2020**, *23*, 101851.

**ADVANCED
SCIENCE NEWS**

www.advancedsciencenews.com

**ADVANCED
MATERIALS**

www.advmat.de

[37] J. Alcaraz, R. Xu, H. Mori, C. M. Nelson, R. Mroue, V. A. Spencer, D. Brownfield, D. C. Radisky, C. Bustamante, M. J. Bissell, *EMBO J.* **2008**, *27*, 2829.

[38] N. Brandenberg, S. Hoehnel, F. Kuttler, K. Homicsko, C. Ceroni, T. Ringel, N. Gjorevski, G. Schwank, G. Coukos, G. Turcatti, M. P. Lutolf, *Nat. Biomed. Eng.* **2020**, *4*, 863.

[39] S. Decembrini, S. Hoehnel, N. Brandenberg, Y. Arsenijevic, M. P. Lutolf, *Sci. Rep.* **2020**, *10*, 10275.

[40] K. Achberger, C. Probst, J. Haderspeck, S. Bolz, J. Rogal, J. Chuchuy, M. Nikolova, V. Cora, L. Antkowiak, W. Haq, N. Shen, K. Schenke-Layland, M. Ueffing, S. Liebau, P. Loskill, *Elife* **2019**, *8*, e46188.

[41] M. A. Lancaster, J. A. Knoblich, *Nat. Protoc.* **2014**, *9*, 2329.

[42] R. P. von Metzen, T. Stieglitz, *Biomed. Microdevices* **2013**, *15*, 727.

[43] R. M. Wright, K. T. Ramesh, *Biomech. Model. Mechanobiol.* **2012**, *11*, 245.

[44] H. Hertz, *J. Reine Angew. Math.* **1882**, *92*, 156.

[45] J. Rheinlaender, A. Dimitracopoulos, B. Wallmeyer, N. M. Kronenberg, K. J. Chalut, M. C. Gather, T. Betz, G. Charras, K. Franze, *Nat. Mater.* **2020**, *19*, 1019.

[46] S. Budday, R. Nay, R. de Rooij, P. Steinmann, T. Wyrobek, T. C. Ovaert, E. Kuhl, *J. Mech. Behav. Biomed. Mater.* **2015**, *46*, 318.

[47] N. Antonovaite, S. V. Beekmans, E. M. Hol, W. J. Wadman, D. Iannuzzi, *Sci. Rep.* **2018**, *8*, 12517.

[48] N. Guz, M. Dokukin, V. Kalaparthi, I. Sokolov, *Biophys. J.* **2014**, *107*, 564.

[49] Y. M. Efremov, T. Okajima, A. Raman, *Soft Matter* **2020**, *16*, 64.

[50] A. Sales, A. W. Holle, R. Kemkemer, *Soft Matter* **2017**, *13*, 5158.

[51] Y. Zhu, L. Wang, F. Yin, Y. Yu, Y. Wang, M. J. Shepard, Z. Zhuang, J. Qin, *Integr. Biol.* **2017**, *9*, 968.

[52] A. A. Rauscher, M. Gyimesi, M. Kovacs, A. Malnasi-Csizmadia, *Trends Biochem. Sci.* **2018**, *43*, 700.

[53] A. Petrosyan, C. A. Casey, P. W. Cheng, *Sci. Rep.* **2016**, *6*, 31962.

[54] J. Haorah, D. Heilman, B. Knipe, J. Chrastil, J. Leibhart, A. Ghorpade, D. W. Miller, Y. Persidsky, *Alcohol. Clin. Exp. Res.* **2005**, *29*, 999.

[55] J. C. Martens, M. Radmacher, *Pflugers Arch* **2008**, *456*, 95.